Electronic Supplementary Material (ESI) for Energy & Environmental Science.
This journal is © The Royal Society of Chemistry 2023

Supplementary Information

Reversible light degradation in organic photovoltaics induced by long-persistent radicals

Difei Zhang,‡[a] Chao Liu,‡[b,c] Kaicheng Zhang,[b] Yanhua Jia,[a] Wenkai Zhong,[a] Weidong Qiu,[a] Yuanfeng Li,[a] Thomas Heumüller,[b,c] Karen Forberich,[b,c] Vincent M. Le Corre,[b] Larry Lüer, [b] Ning Li*[a,b,c,d], Fei Huang,*[a,d] Christoph J. Brabec,[b,c] Lei Ying*[a]

[a] Institute of Polymer Optoelectronic Materials and Devices, State Key Laboratory of Luminescent Materials and Devices, South China University of Technology, Guangzhou 510640, P. R. China. E-mail: ningli2022@scut.edu.cn, msfhuang@scut.edu.cn, msleiying@scut.edu.cn

[b] Institute of Materials for Electronics and Energy Technology (i-MEET), Friedrich-Alexander-University Erlangen-Nürnberg, Erlangen 91058, Germany

[c] Helmholtz Institute Erlangen-Nu¨rnberg for Renewable Energy (HI ERN), Forschungszentrum Jülich GmBH, Erlangen 91058, Germany

[d] Pazhou Lab, Guangzhou, 510320, China† Electronic supplementary information (ESI) available.

‡ D. Z. and C. L. contributed equally to this work.

Experimental Section

Materials.

PTzBI-dF was synthesized according to the literatures. Y6-BO was purchased from Dongguan Volt-Amp Optoelectronics Tech. Co. Ltd. (Dongguan, China). ZnO NPs (Product N-10) was received from Avantama. 2PACz, MoO_x and o-xylene was purchased from Sigma Aldrich. All the materials were used as received.

Device fabrication.

All the OSC devices were fabricated with inverted device structure in i-MEET, FAU. ZnO NPs was spin-coated on precleaned ITO substrates for 3000 rpm followed by thermal annealing in air at 200 °C for 60 min. Afterwards, the substrates were transferred to N_2 glovebox. PTzBI-dF:Y6-BO (1:1, wt) blend solvent with polymer concentration of 9.5 mg mL^{-1} in o-xylene was stirred at 80 °C for 2 h in glovebox. The warm blend solvents were spin-coated on ZnO layer to obtain active-layer thickness from 90 to 130 nm, followed by thermal annealing at 110 °C for 10 min in glovebox. Finally, 10 nm MoO_x and 100 nm Ag were deposited atop in vacuum chamber at a pressure about 1×10^{-6} mbar though a mask with open area of 0.104 cm^2. Electron-only (ITO/ZnO/Active layer/PFN-Br/Ag) and hole-only (ITO/2PACz/Active layer/MoO_x/Ag) devices for SCLC measurement and driving voltage measurement were prepared with the same method.

OSCs characterization and stability measurement.

All the device characteristic were tested in air. *J-V* curves were obtained by a Keithley 2400, with AM1.5G illumination at 100 mW cm^{-2} provided by a solar simulator (Oriel Sol 1A, from Newport), and J_{SC} were verified by EQE. EQE spectra were obtained from an integrated system from Enlitech (QE-R), Taiwan. For stability measurements, devices were placed in N_2 chamber, and illumination was provided by LED (wavelength 400~700 nm), with light intensity adjusted to ensure the J_{SC} of each device equivalent to measured J_{SC} under AM1.5G. Unless state otherwise, all the standard stability measurements were under open-circuit mode, with active layer thickness of 90 nm. Thermal annealing treatments for reversible process were done in the N_2 chamber or N_2 glovebox at dark.

In-situ absorption and morphology characteristic.

In-situ absorption spectra were conducted by a SpectraMax M2 Platereader from 300 to 990 nm in 6 nm steps with an integrated x-y stage for distinct spots on AMADA (Autonomous Materials and Device Application Platform) in N_2.[1] The thickness of the films was measured by the Tencor Alpha Step D 100 surface profiler. GIWAXS measurements were conducted on the beam line 7.3.3 of the Advanced Light Source (ALS) at the Lawrence Berkeley National Laboratory (LBNL) in the United States. Pixel size of 0.172 mm × A 0.172 mm 2D charge coupled device detector was used to image scattered signals in a helium atmosphere. The thin film samples were spin-coated on Si/PEDOT: PSS substrates. The preparation process of all the samples was consistent with OSCs, with TA at 110 °C/10 min for active layers.

Transient measurements and light intensity dependence.

For TPV measurement, a white light LED was used as background. A second 405 nm laser diode was driven by a waveform generator Agilent 33500B and a highly linear photodiode, in order to keep the J_{SC} for OSC similar to the one obtained from AM1.5G. The light intensity was allowed to reproducibly adjust over a range of 0.1~4 suns with error below 0.5%. A small perturbation was induced with the 405 nm laser diode, and the intensity of the short (50 ns) laser pulse was adjusted to keep the voltage perturbation at about 5 mV. V_{OC} was measured with an Oscilloscope (Tekronix MDO 3024). The voltage would decay back to steady-state value with a single exponential decay after the pulse, and the characteristic decay time was calculated by linear fitting of logarithmic plot of the voltage transient and returned the small perturbation charge carrier lifetime. Light intensity dependence measurements were conducted with the calibrated 405 nm laser, and recorded the device parameters under different light intensities. For CE measurement, the 405 nm laser pulse illuminate the OSC for 200 μs, driving the cell to a steady open-circuit mode, and the device was switched to short-circuit mode (50 Ω) at the end of illumination within 50 ns. For photo-CELIV measurement, OSCs was illuminated by the 405 nm laser pulse, and the current transients were recorded after series of delay time across an internal 50 Ω resistor of an oscilloscope (Agilent Technologies DSO-X 2024A). The ramp was 60 μs long and 3 V in amplitude and set to start with an offset matching the V_{OC} of the cell for each delay time. By recording Δj and j(0), dynamic device mobility was calculated as

$$\mu = \frac{2d^2}{3At_{max}^2\left[1 + 0.36\frac{\Delta j}{j(0)}\right]}$$

where $t_{\max}$ is the time corresponding to the maximum of the photo-CELIV trace, d is active layer thickness, the rise speed of the voltage A = dU/dt. The thickness in the measurements was about 100 nm, and the maximum voltage was 3 V, resulting in the maximum electric field of 3×10^5 V cm^{-1}.

Simulations.

J-V and EQE simulations were accomplished by commercially available software SETFOS based on drift-diffusion model. Initial setting could be found in Table S3. A basic device structure was described by the refractive index n, extinction index k, dielectric constant, energy levels and effective charge density of states for different layers (Table S3, ESI†). The n and k values were determined from transmission measurements based on a method published by Kerremans et al.[2] Because we did not observe prominent changes in shunt resistance (R_{sh}) and series resistance (R_s) for stability testing devices (Table S2, ESI†), we used fixed measured values from a fresh device in the entire process to reduce the number of independent variables.

Impedance and driving voltage measurements.

Impedance measurements were conducted on Zahner Zennium Pro potentiostat in N_2 glovebox, with a perturbation of amplitude 20 mV and frequency of 5 kHz. The voltage driving measurement was performed in N_2 glovebox, and used a Keithley 2400 source meter to provide constant output current of 1 mA and record the driving voltage under alternating AM 1.5G illumination and dark conditions. For electron-only devices, measurement were begin after the first 30 s illumination for ZnO surface defects passivation. It is noted that the initial dark voltage value of electron-only device was significantly higher than that of the hole-only device; and the dark voltage value decreased after pre-illumination for approximately 30 s because of the filling of surface defects at the ZnO interface.

EPR measurement.

EPR was performed on the Bruker Electron Paramagnetic Resonance Spectrometer E500-10/12. Samples preparation: 2mg of PTzBI-dF:Y6-BO (1:1, wt: wt) or PM6:Y6-BO (1:1, wt: wt) was dissolved in *o*-xylene with a total concentration of 20 mg mL^{-1}, and stirred at 100 °C for about 2 hours. The solvents were added to NMR tubes, cooled to room temperature and dried with a vacuum

pump (1×10^{-4} pa). The ageing samples were exposed to AM 1.5G solar simulator for about 20 hours, and TA samples were heated in oil bath at 110 °C for 10~20 min. The strength of signals was closely related to sample fabrication process and blending morphology.

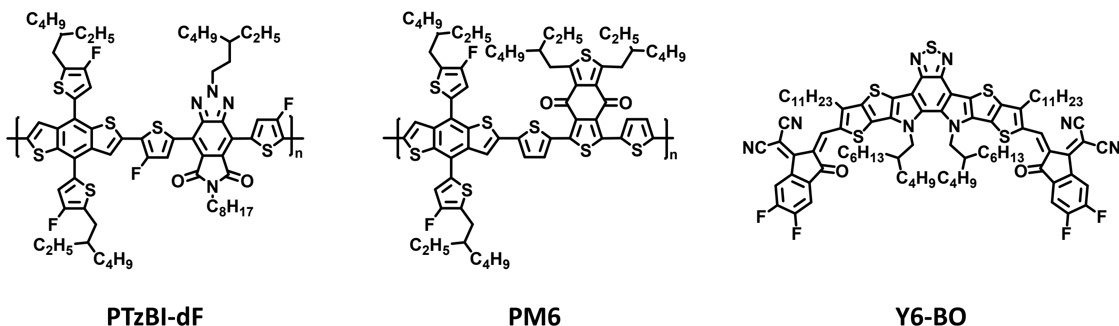

Figure S1. The chemical structures of photovoltaic materials involved in this work.

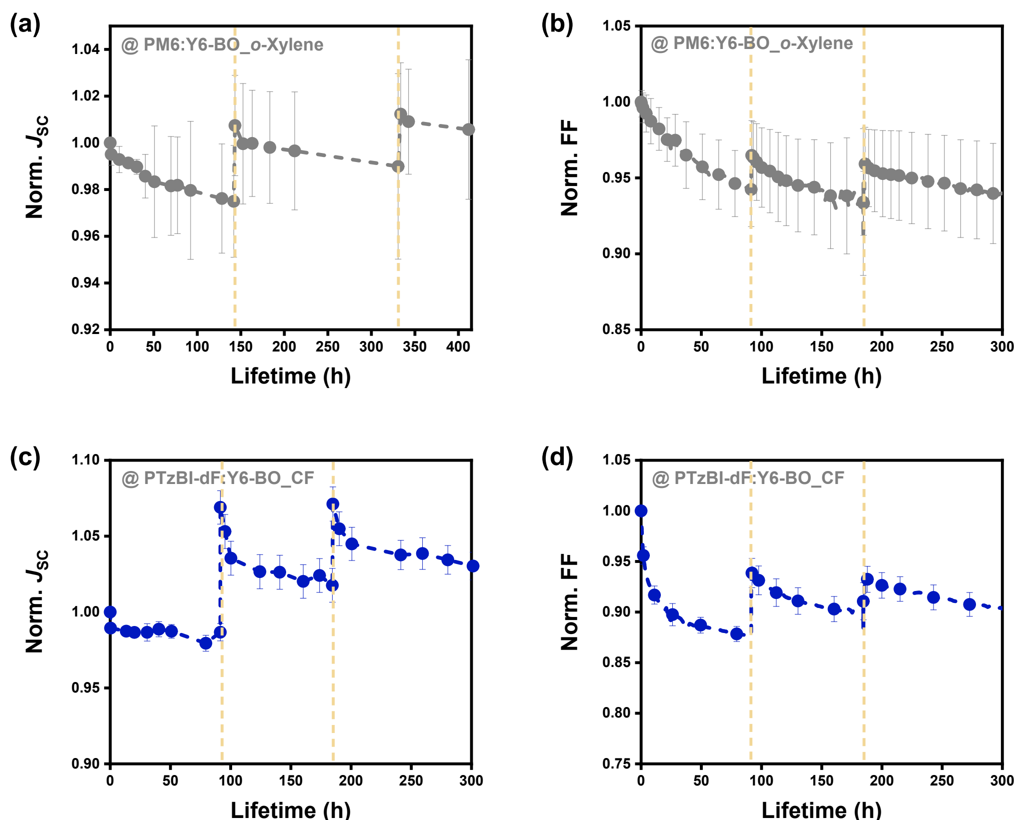

Figure S2. The evolution of device stability under 1 sun illumination: (a) Normalized J_{SC} degradation and (b) FF degradation for TA devices based on PM6:Y6-BO system processed by *o*-xylene. (c) Normalized J_{SC} degradation and (d) FF degradation for post-TA devices based on PTzBI-dF:Y6-BO system processed by CF. Yellow dashed lines represent in situ TA treatments at 110 °C for 10 min in nitrogen.

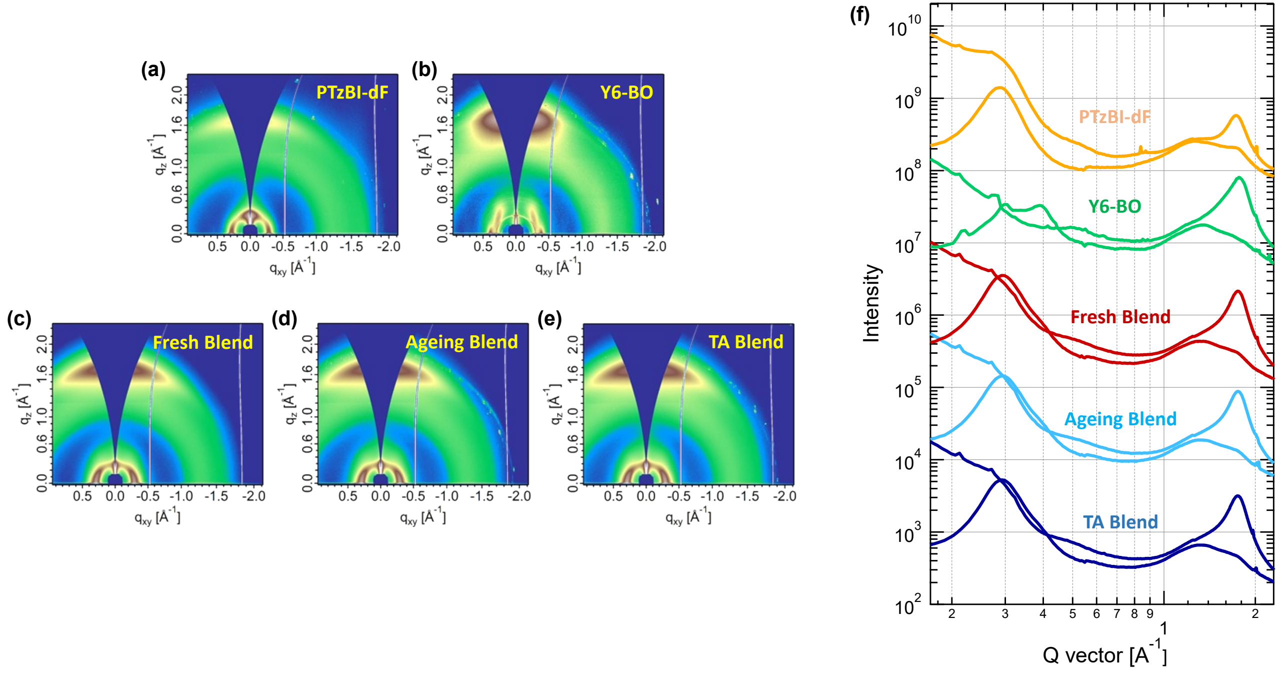

Figure S3. 2D GIWAXS pattern for (a) PTzBI-dF pure film, (b) Y6-BO pure film, (c) fresh, (d) ageing and (e) TA PTzBI-dF:Y6-BO blend films. (f) Integrated scattering profiles for the corresponding films. Solid lines refer to OOP direction, and dashed lines refer to IP direction.

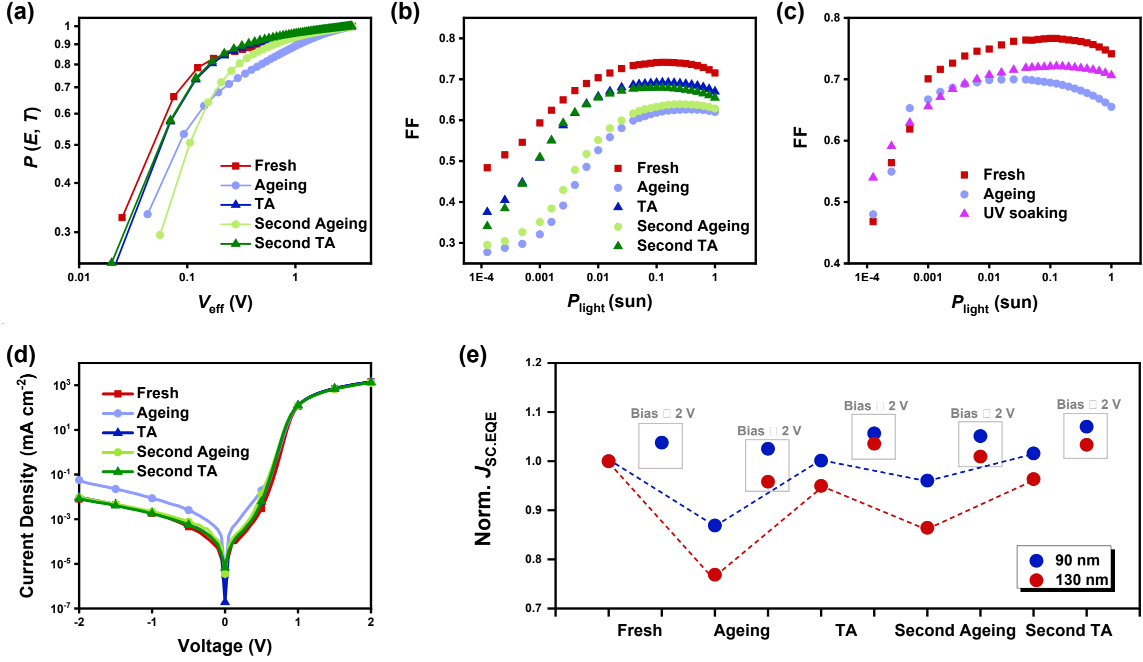

Figure S4. (a) Charge dissociation probability $P(E, T)$ versus V_{eff}. (b) P_{light}—FF dependence for device with post-TA treatment. (c) P_{light}—FF dependence for device with 365 nm wavelength UV exposure for 1 min. (d) Dark J—V characteristic. (e) J_{SC} integrated by EQE measurement on devices with different active layer thicknesses and normalized to initial value; grey boxes represent the maximum photo-generated current density integrated by EQE applying -2 V bias.

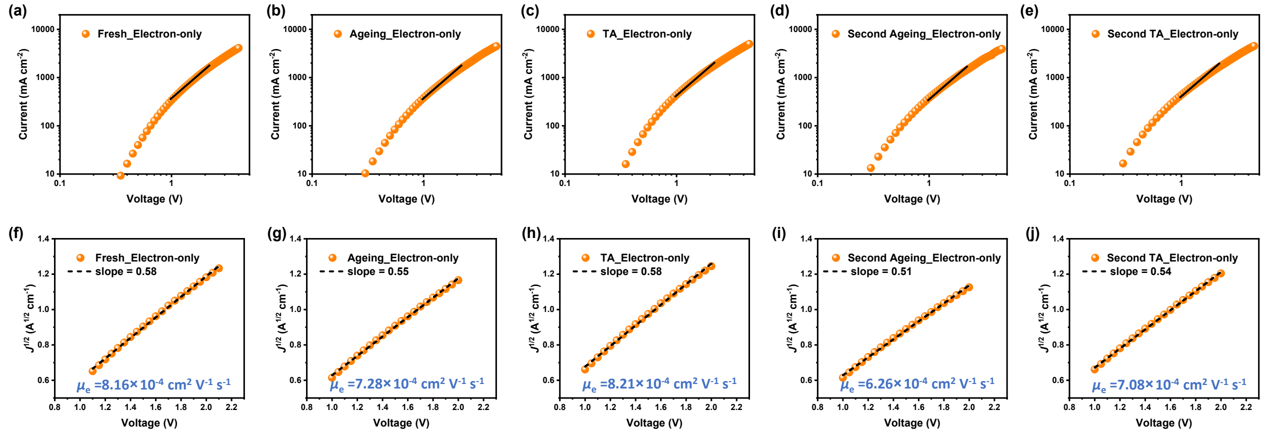

Figure S5. Electron mobility of electron-only devices measured by SCLC method for PTzBI-dF:Y6-BO system. The black solid lines with slope of 2 in (a-e) are guide to the eye, and dashed lines in (f-j) are linear fitting.

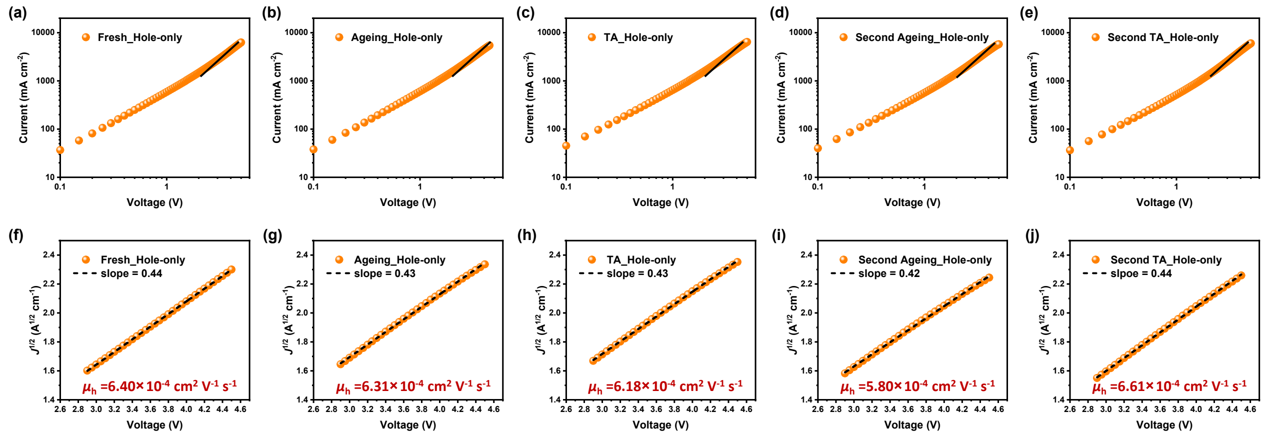

Figure S6. Hole mobility of hole-only devices measured by SCLC method for PTzBI-dF:Y6-BO system. The black solid lines with slope of 2 in (a-e) are guide to the eye, and dashed lines in (f-j) are linear fitting.

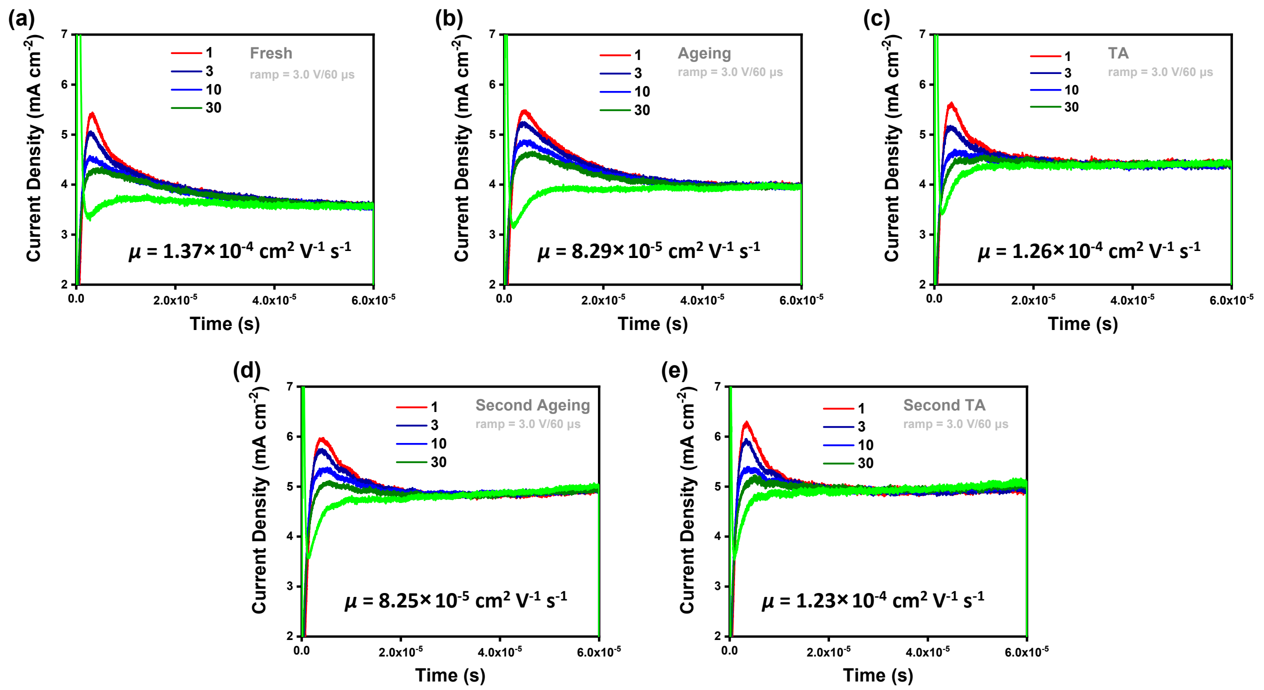

Figure S7. Dynamic device mobility of OSCs measured by photo-CELIV method for PTzBI-dF:Y6-BO system. Colored lines represent different decay time (μs). Ramp was set as 60 μs/3 V, and the mobilities were calculated by decay time of 1 μs.

Table S1. SCLC mobility and photo-CELIV dynamic device mobility.

Measuring Method		Fresh (cm^2 V^{-1} s^{-1})	Ageing (cm^2 V^{-1} s^{-1})	TA (cm^2 V^{-1} s^{-1})	Second Ageing (cm^2 V^{-1} s^{-1})	Second TA (cm^2 V^{-1} s^{-1})
Photo-CELIV	**device**	1.37×10^{-4}	8.29×10^{-5}	1.26×10^{-4}	8.25×10^{-5}	1.23×10^{-4}
SCLC	μ_e	8.16×10^{-4}	7.27×10^{-4}	8.20×10^{-4}	6.25×10^{-4}	7.08×10^{-4}
	μ_h	6.40×10^{-4}	6.31×10^{-4}	6.18×10^{-4}	5.78×10^{-4}	6.61×10^{-4}

Table S2. Series resistance and shunt resistance under AM 1.5G and dark.

Condition	Process	R_{series} (Ω)	R_{shunt} (Ω)
AM 1.5G	**Fresh**	0.683	1.42×10^{3}
	Ageing	0.718	1.58×10^{3}
	TA	0.706	8.50×10^{2}
	Second Ageing	0.809	6.49×10^{2}
	Second TA	0.767	8.23×10^{2}
Dark	**Fresh**	0.712	1.31×10^{5}
	Ageing	0.715	1.63×10^{4}
	TA	0.713	9.97×10^{5}
	Second Ageing	0.79	6.83×10^{5}
	Second TA	0.766	1.03×10^{6}

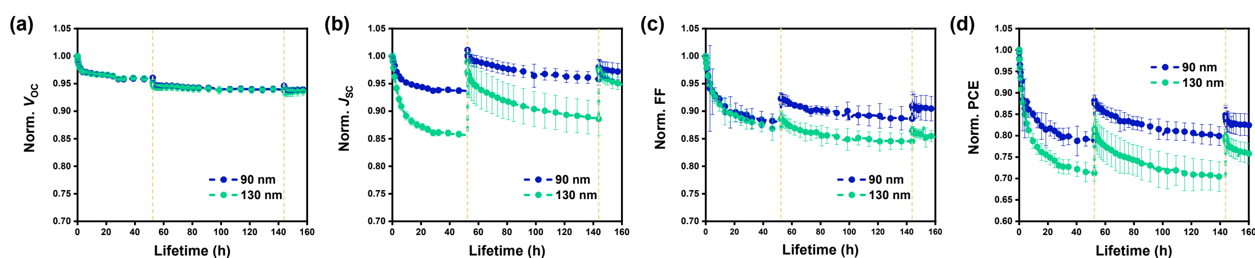

Figure S8. The evolution of device stability under 1 sun illumination with different active layer thicknesses: (a) Normalized V_{OC}, (b) normalized J_{SC}, (c) normalized FF and (d) normalized PCE degradation for devices. Yellow dashed lines represent in situ TA treatments at 110 °C for 10 min in nitrogen. PTzBI-dF:Y6-BO system was processed by *o*-xylene, and devices were under open-circuit mode.

Table S3. Basic settings for SETFOS.

<table>
<tr><th>Electrode/Interface</th><th>Active Layer</th><th>Drift-diffusion Setting</th></tr>
<tr>
<td>ITO：
• Thickness = 120 nm
• E_F = -4.3 eV

Ag：
• Thickness = 100 nm
• E_F = -5.3 eV

ZnO:
• Thickness = 30 nm
• HOMO -7.0 eV，N_0 = 3.7E24 m^{-3}
• LUMO -4.3 eV，N_0 = 3.7E24 m^{-3}
• Dielectric constant = 8.5
• μ_e = 1E-6 m^2 V^{-1} s^{-1}
• μ_h = 1E-7 m^2 V^{-1} s^{-1}

MoO_x:
• Thickness = 10 nm
• HOMO -5.3 eV，N_0 = 1E24 m^{-3}
• LUMO -2.21 eV，N_0 = 1E24 m^{-3}
• Dielectric constant = 10
• μ_e = 1E-5 m^2 V^{-1} s^{-1}
• μ_h = 1E-3 m^2 V^{-1} s^{-1}</td>
<td>Semiconducting:
• Thickness = 110 nm
• HOMO -5.51 eV，N_0 = 7E27 m^{-3}
• LUMO -4.1 eV，N_0 = 7E27 m^{-3}
• Dielectric constant = 3.5
• Optical generation efficiency = 0.9
• Langevin recombination efficiency = 0.001
• μ_e = 8.6E-8 m^2 V^{-1} s^{-1}
• μ_h = 6.4E-8 m^2 V^{-1} s^{-1}

Absorption settings：
• Sweeping wavelength 300~1000 nm
• Illumination spectrum AM 1.5G

Electron trap density in our model：
• Trap energy depth = 0.5 eV
• Electron capture rate = 1E-8 cm^3 s^{-1}
• Hole capture rate = 1E-16 cm^3 s^{-1}

Hole trap density in our model：
• Trap energy depth = 0.5 eV
• Electron capture rate = 1E-16 cm^3 s^{-1}
• Hole capture rate = 1E-8 cm^3 s^{-1}</td>
<td>Physical settings：
• Temperature = 300 K
• Trapping
• SRH recombination

Electrical circuit：
• Device area = 1 cm^2
• R_s = 0.92 Ω
• R_{sh} = 800 Ω</td>
</tr>
<tr><th colspan="3">Standard output for device performances (initial state)</th></tr>
<tr><td colspan="3">• V_{OC} = 0.8465 V • J_{SC} = 25.07 mA cm^{-2} • FF = 0.7647 • PCE = 16.23%</td></tr>
</table>

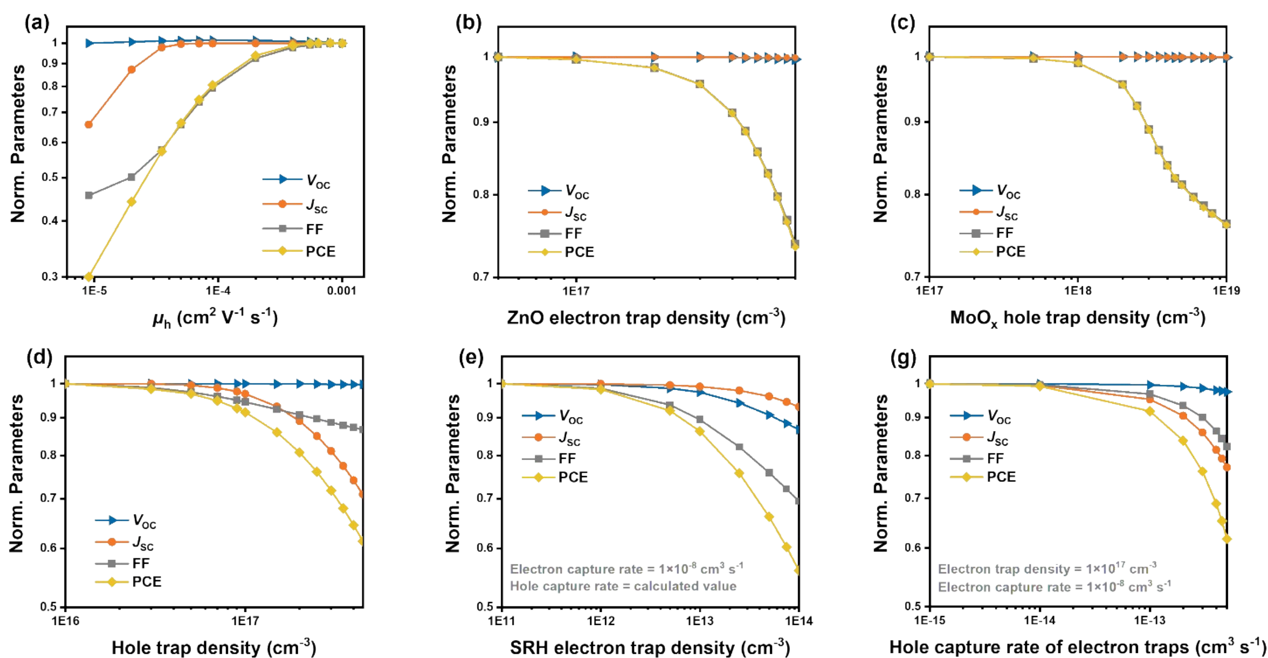

Figure S9. Drift-diffusion simulations of normalized devices parameters. (a) Hole mobility. (b) Electron trap density in ZnO layer. (c) Hole trap density in MoO_x layer. (d) Hole trap density in active layer with our recombination model. (e) Electron trap density in active layer with typical SRH recombination model. Electron capture rate was set as 1×10^{-8} cm^3 s^{-1}, and hole capture rate was calculated according to the model, close to 1×10^{-8} cm^3 s^{-1}. (f) Hole capture rate of electron traps. Electron trap density was set as 1×10^{17} cm^3 s^{-1}, and electron capture rate was set as 1×10^{-8} cm^3 s^{-1}. When hole capture rate was set as 0, the results were equal to the results from mono-molecular recombination model.

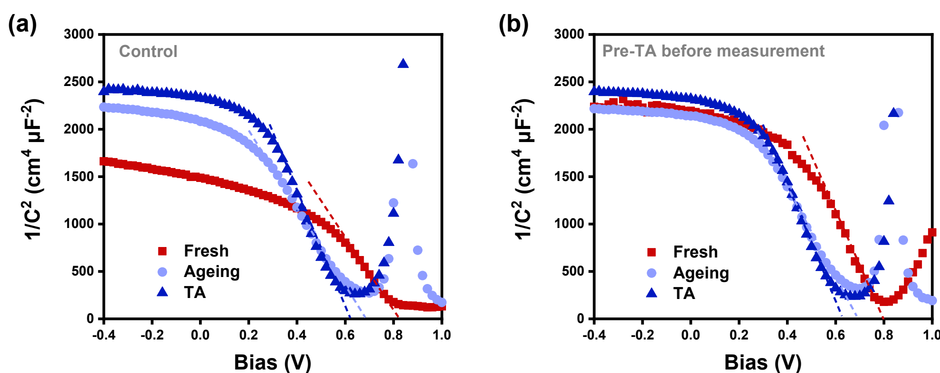

Figure S10. $C-V$ dependence of (a) control device and (b) pre-TA device.

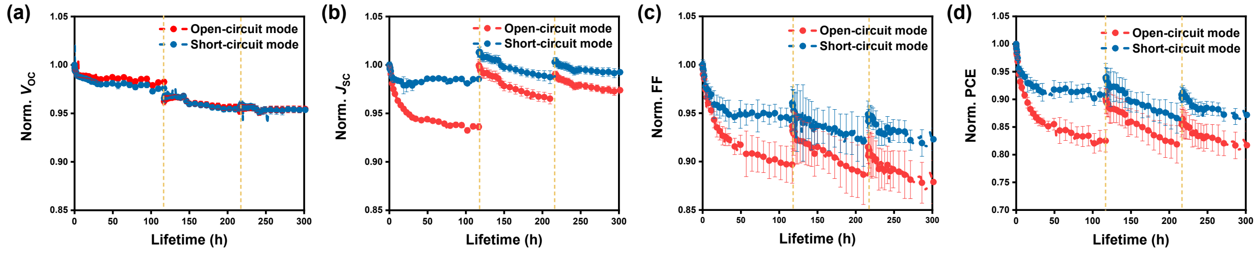

Figure S11. The evolution of device stability under 1 sun illumination with different external loads: (a) normalized V_{OC}, (b) normalized J_{SC}, (c) normalized FF and (d) normalized PCE degradation. Yellow dashed lines represent in situ TA treatments at 110 ℃ for 10 min in nitrogen. PTzBI-dF:Y6-BO system was processed by *o*-xylene, and active layer thickness was about 90 nm.

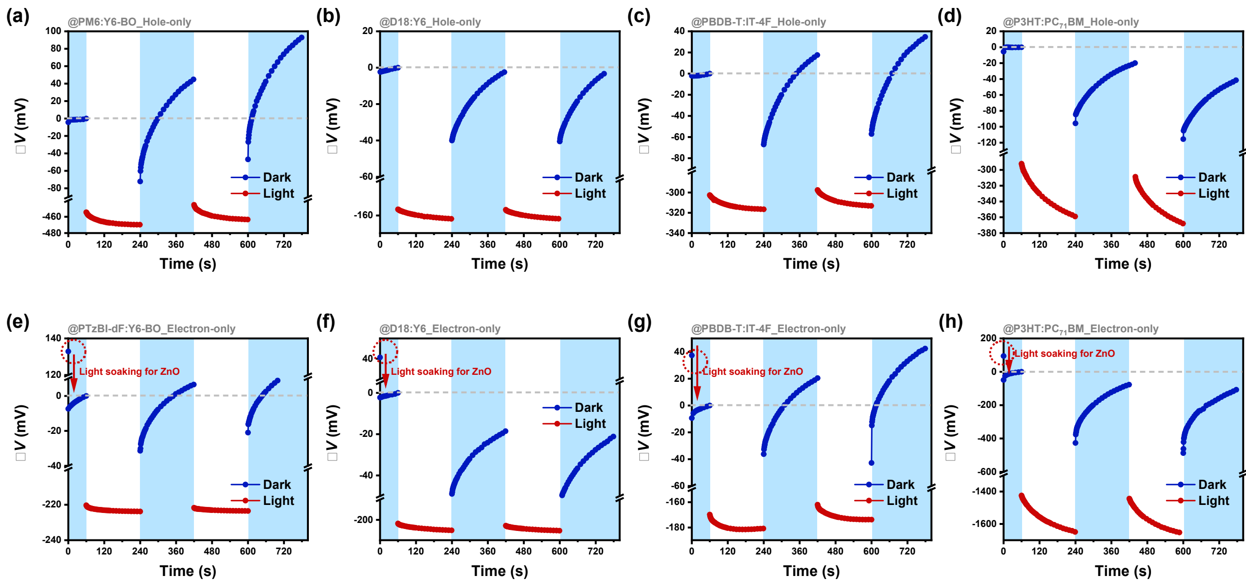

Figure S12. Driving voltage measurements under constant current 1 mA: (a-d) Hole-only devices and (e-h) electron-only devices for different OPV material systems. Red arrow represents light soaking for passivation of surface defects in ZnO. Blue areas represent measurements in dark, white areas represent measurements under AM 1.5G, and grey dashed lines guiding to the initial voltage.

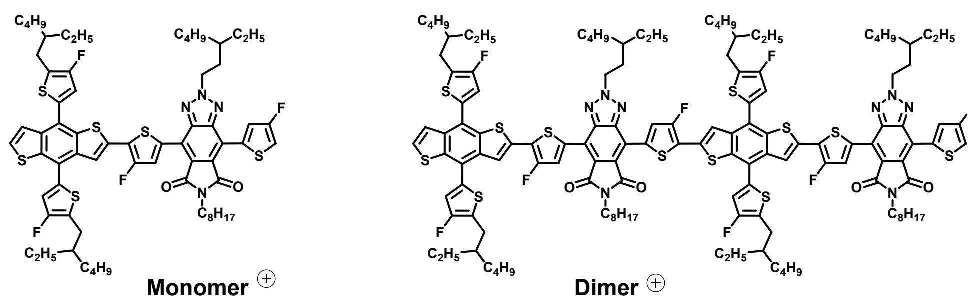

Figure S13. PTzBI-dF monomer and dimer model for DFT calculation.

Table S4. DFT calculation on B3LYP/6-31G*.

Geometry	Neutral *E(B3LYP)(au)	Cation *E(B3LYP)\(au/Hatree)	λ (Hartee)	λ (eV)	λet (eV)
Monomer	-4618.9206	-4618.9161	0.0044	0.1206	-
Monomer_Cation	-4618.6854	-4618.6905	0.0051	0.1389	0.2595
Dimer	-9236.6586	-9236.6560	0.0026	0.0713	-
Dimer_Cation	-9236.4408	-9236.4438	0.0030	0.0808	0.1521

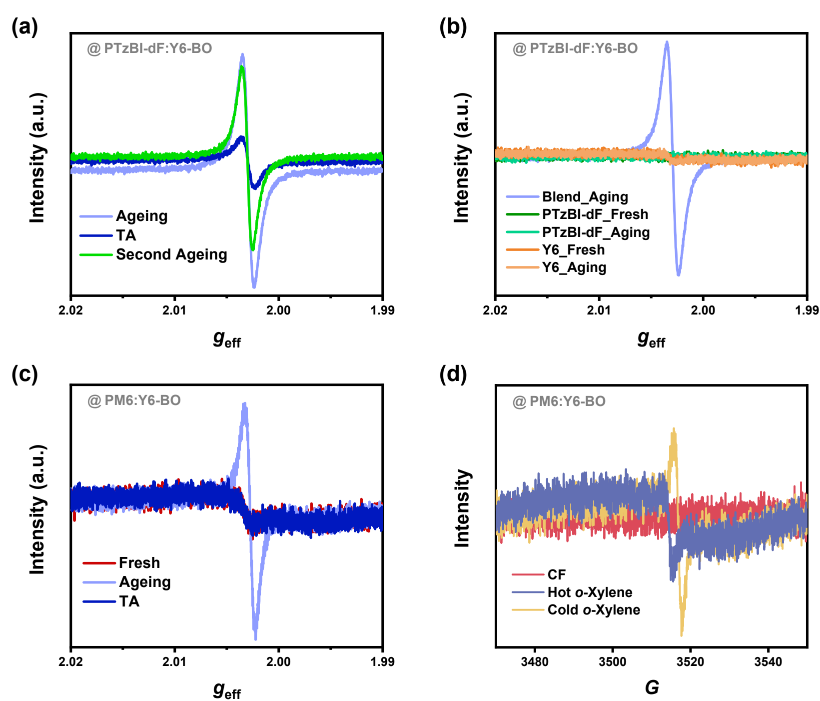

Figure S14. EPR measurements: (a) Second light ageing process for PTzBI-dF:Y6-BO blend. (b) Comparison among pristine PTzBI-dF, pristine Y6-BO and PTzBI-dF:Y6-BO blend. (c) PM6:Y6-BO blend. (d) PM6:Y6 blend processed with different solvents and conditions.

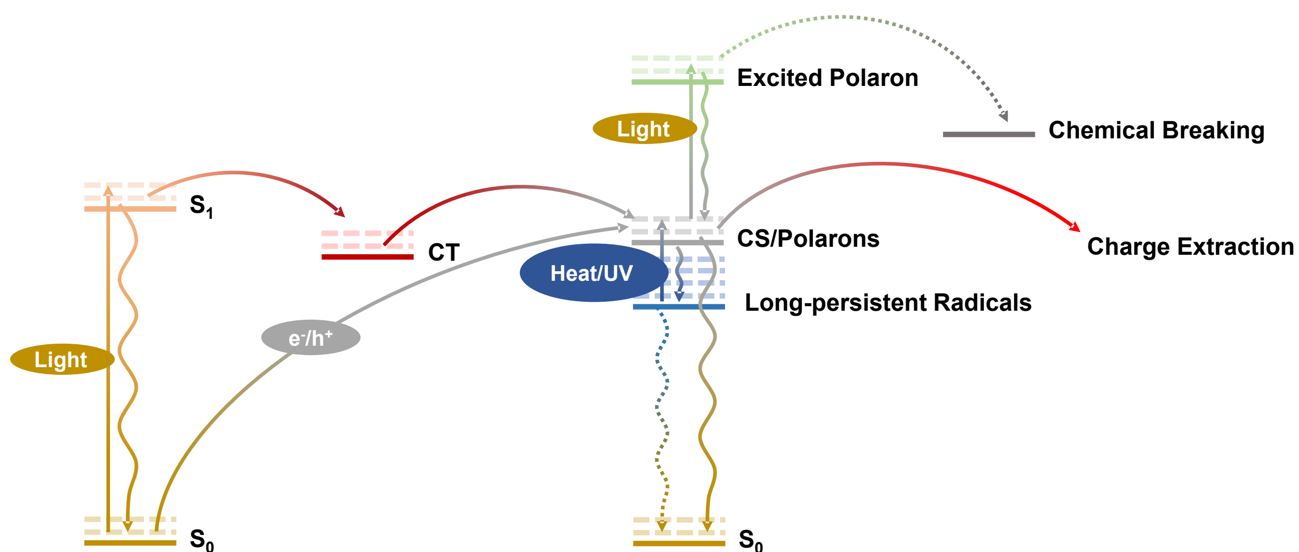

Figure S15. Formation, release and recombination process of light-induced long-persistent radicals in OSCs.

References

1 J. Wagner, C. G. Berger, X. Du, T. Stubhan, J. A. Hauch and C. J. Brabec, *J. Mater. Sci.*, 2021, **56**, 16422-16446.

2 R. Kerremans, C. Kaiser, W. Li, N. Zarrabi, P. Meredith and A. Armin, *Adv. Opt. Mater.*, 2020, **8**, 2000319.